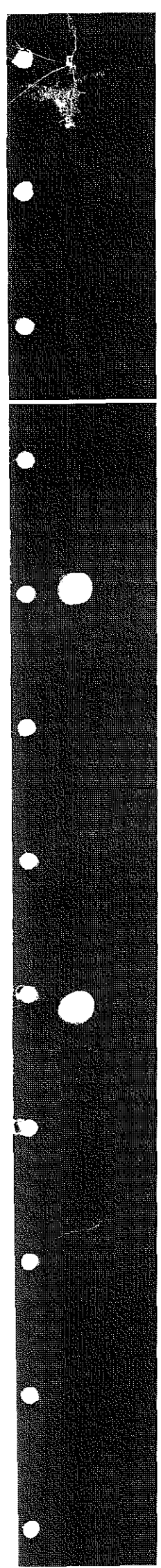

Some Aspects of Hot Cell Mechanical Testing at AEA Technology plc

Annual Meeting of the European Working Group
'Hot Laboratories & Remote Handling'
ECN, Petten, The Netherlands
May 14-15, 1996

JS Dakin, JAM Douglas & JG Gravenor

AEA Technology

ANNUAL MEETING OF THE

EUROPEAN WORKING GROUP

'HOT LABORATORIES AND

REMOTE HANDLING'

ECN, PETTEN, THE NETHERLANDS

MAY 14-15, 1996

Some Aspects of Hot Cell Mechanical Testing at AEA Technology plc

by

J S Dakin
J A M Douglas
J G Gravenor

Some Aspects of Hot Cell Mechanical Testing at AEA Technology plc

by

J S Dakin, J A M Douglas and J G Gravenor

INTRODUCTION

The mechanical properties of irradiated fuel cladding and components continue to be of importance in the nuclear industry with respect to improved fuel utilisation and more flexible plant operation in both water-cooled and gas-cooled thermal reactor systems. Progress towards higher burnup and improved load following place greater demands on the mechanical properties if higher levels of safe fuel performance are to be demonstrated. Data from post-irradiation testing of spent fuel and components is therefore an essential input into codes which are used to support safety case submissions to regulatory authorities. The comprehensive services provided by the Fuel Performance Group of AEA Technology plc to nuclear utilities include a variety of mechanical testing techniques and testpiece machining capabilities for irradiated fuel and components together with data assessment services. In this paper a few examples illustrating the range of testing investigations are described

Biaxial Stress Testing of LWR Cladding

Metals subjected to biaxial stress generally show increased yield strength and reduced ductility. These effects can be more pronounced in anisotropic materials and are related to the variation of yield strength with crystallographic orientation. Zircaloy cladding is anisotropic owing to the texture produced during manufacture, and is subject to biaxial loading in service by the combined effects of coolant pressure, thermal expansion of the fuel pellets or by swelling. Post-irradiation tests under various biaxial stress conditions are desirable in order to fully characterise the yield strength and ductility of the material, and to fulfil this requirement a facility for biaxial tests on cladding has been developed.

Equipment

The main features are shown in Figure 1 and comprise the following:

servohydraulic mechanical testing machine
in-cell and out-of-cell hydraulic pressure circuit
hydraulic pressure supply system
low pressure air system
instrumentation and control

The mechanical testing machine is housed in a shielded cell (200mm thick lead shielding) and is used to apply the axial force to the testpiece. The machine is under computer control and applies a tensile or compressive axial force which is set to a pre-determined proportion of the hydraulic pressure; thus the ratio of the hoop stress to the axial stress (the biaxial ratio) is maintained constant throughout a test. The pressurising head to which the testpiece is attached fits directly into the testing machine upper

hydraulic grip and is connected to the hydraulic supply. The crosshead is maintained in a fixed position when the biaxial testing assembly and its pipework is installed. The bottom end of the testpiece is held in the lower grip which is attached to the actuator, and which in turn applies the axial force. When not in use the biaxial testing facility can then be easily removed from the testing machine and stored, and the testing machine used for other purposes.

The pressure supply system consists of an air-hydro pump, driven by compressed air, which pumps hydraulic fluid (Dow-Corning 710) from a heated reservoir to charge an pneumatic-hydraulic intensifier. The intensifier has a pressure ratio of 10:1 and is driven by a 17 MPa gas bottle supply so it can deliver a maximum hydraulic pressure of 170 MPa, which is sufficient to burst the highest yield strength cladding. The pressurisation rate is controlled by a flow control orifice included in the gas supply line. Warming and recirculation of the hydraulic fluid before the test is carried out to remove any air, this is important to avoid any explosive effect when the testpiece bursts which would scatter oil and contamination over the cell interior. The testpiece extension is measured by axial and diametral extensometers. The axial extensometer is a standard clip-on type with a gauge length of 50 mm while the diametral extensometer is a modified axial type with extension arms which contact the cladding wall at its central point. The diametral extensometer is supported externally on the furnace assembly. The maximum test temperature is 400°C.

The testpieces were approximately 300mm long with steel end fittings swaged to the top and bottom; the top fitting had a central hole to allow fluid to pass into the testpiece (Figure 2), the bottom fitting had a steel extension rod for attachment to the lower grip. A filler rod was placed in the testpiece bore to reduce the volume of hydraulic fluid required.

Biaxial Test Results

The test results comprised a plot of pressure against axial and diametral extension. An example of the data obtained for an applied axial force to hydraulic axial force ratio of 1.5 is shown in Figure 3. The 0.2% proof stress in the axial and diametral directions was calculated using the following relations:

$$\sigma_h = Pr/t$$
$$\sigma_{ap} = Pr/2t$$
$$\sigma_{af} = F/2\pi rt$$
$$\sigma_a = \sigma_{ap} + \sigma_{af}$$

where σ_h = hoop stress, σ_{ap} = axial stress due to internal pressure, σ_{af} = axial stress due to applied axial force, P = pressure, F = applied axial force, r = cladding tube radius, t = cladding thickness. The axial stress is determined by the sum of the hydraulic pressure component and the force applied by the testing machine. Therefore to give "closed end" burst conditions, the force applied by the testing machine is zero, while to obtain "open end" burst conditions the force applied by the testing machine is equal and opposite to that generated by the internal pressure (ie $\sigma_{ap} = -\sigma_{af}$) and the resultant axial stress is zero.

For plane strain conditions in an isotropic material $\sigma_h = 2\sigma_a$, which corresponds to closed end conditions. For zircaloy cladding a closed end test does not correspond exactly to plane strain conditions and a range of hoop and axial stress ratios must be examined to determine the point where plane strain deformation occurs. This series of biaxial tests produces the stress ellipse predicted by the modified form of yield theory appropriate for anisotropic materials.

Iodine Stress Corrosion Cracking Investigations

Stress corrosion cracking (SCC) caused by fission product iodine is believed to be responsible for some kinds of power ramp failures in LWR's, and the effect has been investigated by many workers. In some early studies the concentration of iodine was not defined and the cladding material used was poorly characterised. Most of these investigations have been on unirradiated zircaloy, and it has been clearly established that a threshold concentration of iodine is necessary to produce embrittlement. The threshold varies with test temperature. At 500°C the threshold is about 0.001 $\mu g/mm^3$ increasing to 50$\mu g/mm^3$ at 900°C [1] (expressed as volume concentration). However, the iodine concentrations determined in these tests were well above the amounts of iodine that could be present in the free state inside fuel rods, and this led to doubts whether iodine is in fact responsible for SCC. On the other hand radiolysis of iodine compounds could lead to higher free iodine concentrations than would be predicted from thermodynamic considerations. To help to resolve these problems more data are desirable for SCC in irradiated zircaloy cladding, and so a technique has been developed for performing hot cell SCC tests with controlled quantities of iodine [2].

Equipment

The tests on irradiated zircaloy-2 (irradiated to 24 GWd/tU) were performed in a hot-cell facility which consisted of a specimen mounting frame with provision for gas pressurisation. The specimen test temperature was obtained by electrical resistance heating and was controlled by an infra-red pyrometer focused onto the middle region of the testpiece. End fittings were used of the same design as for the biaxial tests described above, and the fuel was removed using mechanical defuelling techniques. The facility also included two orthogonally mounted real-time X-ray units and fluorescent screens. The X-radioscopic images were used to verify correct operation of the carrier system used to release iodine into the cladding bore. They were also used to estimate the diametral strain which was produced during the tests.

Specimen Preparation

Iodine was introduced into the specimens by enclosing a weighed quantity in a sealed capsule inserted into the cladding bore, which could be opened to release iodine vapour to start the test (Figure 4). The capsule consists of two sections, an inner glass capsule containing the iodine crystals and an outer glass sheath. The open end of the capsule is sealed to a "Sintox" pellet by a halogen-free adhesive and the pellet rests on the outer glass sheath. When the specimen is heated the adhesive degrades, releasing the capsule which falls to the bottom of the glass sheath, so opening it. The iodine crystals vaporise and gaseous iodine passes into the cladding bore through holes in the

glass sheath. The specimen was pressurised using argon from a gas bottle supply, which limited the maximum hoop stress to about 100 MPa; this is too low to produce SCC at operational temperatures of 350°C and consequently these initial investigations were made at 500°C and 600°C, temperatures more typical of fault conditions.

Results of Burst Tests

The effect of iodine in reducing the burst ductility is shown in Figure 5 for a commissioning test at 600°C on unirradiated cladding. A sharp fall in ductility was observed for iodine concentrations of between 7 and 17 $\mu g/mm^2$ and above. The tests on irradiated zircaloy-2 were mainly done at 600°C, with one test at 550°C. The creep deformation of the cladding was measured using the X-radioscopy equipment and is shown in Figure 7, in these short term creep tests the tertiary stage was very prominent. The corresponding ductility data are presented in Figure 7 and although a decrease in ductility is observed at iodine concentrations above 10 $\mu g/mm^2$ (expressed as mass/area) the effect is not so pronounced as for unirradiated cladding, since the ductility of irradiated cladding is only about 20% and is lower than that of unirradiated material even in the absence of iodine. The lower ductility observed is somewhat surprising since rapid annealing of the radiation damage would be expected in tests at 600°C (1h at 500°C is usually sufficient to remove radiation damage structure from irradiated zircaloy). In one test initially done at 500°C for 3h and subsequently increased to 600°C a ductility of 37% was observed which was about twice that of the other 600°C tests, this improved ductility was probably a consequence of radiation damage annealing.

Post Test Examination

Post-test examination was performed to identify the failure type. However, neither the failure type nor the failure site could be identified by visual examination of any of the irradiated specimens. Each specimen was therefore subjected to a simple bubble test by immersion in water and pressurisation with air so that the location of the failure site could be determined. These tests confirmed that in all cases the failure site was adjacent to the iodine carrier in the middle of the testpiece. Some specimens had a faster leak rate than others and an assessment was made of the diameter of the cladding penetration from the records of the rate of pressure loss immediately following failure. The larger failure diameters were probably associated with small tears and the smaller diameters with pinhole failures, but optical re-examination of the identified failure site still did not reveal the defect.

Low Cycle Fatigue Testing with Iodine

Hot cell equipment is currently being assembled to allow tests to be done at higher pressures and therefore at reactor operational temperatures of 350°C. Published data indicates that hoop stresses of about 250 MPa or more are necessary to obtain SCC failures at operational temperature so that the pressure required will be 36 MPa , and to obtain this a gas boost pump and accumulator supply system is being installed. The same capsule technique for introducing controlled quantities of iodine will be employed. Cladding fatigue has assumed increased importance recently for progress

towards improved load following and grid synchronisation characteristics. A further refinement will therefore be the provision of controlled pressurisation rate and venting, so that low-cycle fatigue can be applied to long term tests. The accurate control of the cladding diametral elastic and plastic strain which is required for low-cycle fatigue testing will be achieved by optical strain measurement techniques with a resolution of better than 1 μm.

Fatigue Tests on CAGR Tiebars

A CAGR fuel assembly is held together by a tiebar which passes through guide tubes in the fuel elements, and supports the weight of the stringer during refuelling operations. There is no secondary lifting component and so failure of the tiebar or its end fittings would lead to the stringer being dropped down the fuel channel, with consequential damage and possible overheating of the debris. A very high reliability is therefore required of this component, and accordingly the Nimonic alloy PE16 was selected for its manufacture, as this nickel base superalloy has high creep resistance, excellent strength and ductility, good oxidation resistance and good fabrication characteristics. This alloy has also found application in fast reactor fuels, and has been considered as a candidate plasma containment material for fusion reactors . During service, neutron irradiation can lead to degradation of the mechanical properties and the extent of these effects must be assessed by appropriate post-irradiation examination and testing. The degradation must then be shown not to adversely affect the reliability for on-load refuelling or other fuel handling operations. Probabilistic risk assessment is used for the latter purpose.

The principal mechanical properties measured during post-irradiation examination are the proof stress, ductility, stress rupture strength, slow strain rate strength and high-cycle fatigue. Fatigue is a potential source of deterioration since the tiebar experiences vibration due to coolant flow, which causes wear damage at points of contact with guide tubes, and these wear damaged areas could then in principle act as notches from which fatigue cracks could initiate. Elevated temperature fatigue tests on irradiated tiebar material are described below in which the threshold conditions for crack growth were established and the crack growth properties characterised [3].

Specimen Preparation

The material used was obtained from irradiated tiebars recovered from dismantled spent fuel and was in the form of rod 10.16 mm diameter, originally manufactured from three casts of PE16 alloy by forging, rolling and extrusion. The final heat treatment consisted of solution treatment at 1040°C for 15 minutes followed by ageing at 700°C for 8h to precipitate the γ' phase $Ni_3(Ti,Al)$ which is mainly responsible for the high creep strength of this material. The stringer mean irradiations were 18 to 19 GWd/tU; testpieces were taken from various positions along the bars and so the fast and thermal fluences and the irradiation temperatures varied between different tests, and were evaluated from the reactor operating data. The testpieces were 300 mm long and a slow speed diamond cutting machine fitted with a slitting blade 0.3 mm thick was used to introduce transverse starter notches about 0.8 mm deep having a U-shaped section. The notch width at the mouth was about 0.4 mm and the root radius measured from metallographic sections was 0.15 mm. Using fine glass-insulated alumel wire, two

electrical connections were spot-welded to each side of the notch for crack growth monitoring by the direct current potential difference method. No current supply connections were needed since the testing machine grips were insulated from the load frame and when the specimen was gripped good electrical connection was made automatically. In addition a chromel-alumel (Type K) thermocouple was spot-welded close to the notch for temperature measurement during the fatigue test.

Fatigue Testing Method

The fatigue tests were performed on an Instron shielded servohydraulic testing machine at a frequency of 10 Hz at temperatures from 350°C to 700°C. Since the testpiece was a rod it always had to be maintained under tension to prevent buckling and so a positive R-ratio (minimum load/maximum load) was used of 0.2 . The 10A current for the dcpd crack monitoring was provided by a stabilised power supply unit and a relay unit was used to reverse the direction of current flow at regular intervals, so cancelling thermally generated potentials. The load-shedding method described in the ASTM Standard E647 was used to determine the minimum threshold stress intensity factor range. Crack growth was first initiated by increasing the load range and was then allowed to continue to a depth of about 1 mm before the load shedding procedure was started. Each reduction in the maximum load was 10% or less after crack depth increments of at least twice the plane strain plastic zone size calculated from the relation:

$$r_y = (K_{max}/ \sigma_y)^2/6\pi$$

where r_y is the plastic zone radius (metres) K_{max} is the stress intensity factor at the maximum load ($MN/m^{3/2}$) and σ_y is the proof stress at the test temperature. The proof stress was measured on adjacent testpieces at room temperature using an extensometer to determine the 0.2% plastic strain offset, and the proof stress then estimated at test temperature using an empirical relation for irradiated PE16. The crack growth threshold was considered to be reached when a crack growth rate of less than 10^{-10} m/cycle was demonstrated. Crack growth data were obtained from the initial part of the test over which the stress intensity factor range, ΔK, was increasing.

Determination of Crack Depth and Stress Intensity Factor

Crack depth measurement depended on a known calibration between the dcpd value and depth, and this was determined both experimentally and by calculation. Because of the small dimensions of the specimen and the notch, and the problems of positioning the dcpd leads with manipulators, it was not practicable to use a single calibration curve for all the tests. Instead, an individual calibration curve was determined retrospectively for each test by stopping the fatigue cycling and crack growth before specimen rupture, then measuring the initial and final crack depth after breaking the specimen at room temperature, and interpolating between them. The fatigue crack surface was heat tinted and during optical examination could easily be distinguished from the ductile fracture surface which resulted from breaking at room temperature. An interpolation function was derived from dcpd/crack depth data by marking the fatigue crack surface of an unirradiated specimen at regular intervals by increasing the stress range for a small number of cycles at regular times during the test. This

produced a series of semi-elliptical marks on the thumbnail-shaped fatigue surface, each of which corresponded to a certain number of cycles. An empirical equation was then derived to describe the dcpd/crack depth relationship. Additional confidence in the calibration was provided by 3-dimensional finite element calculation of the potential distribution in a notched and fatigue-cracked testpiece. The stress intensity factor was calculated from a published empirical equation for thumbnail-shaped cracks, and its applicability verified by 3-dimensional finite element calculation.

Fatigue Test Results

The data were presented in the log crack growth rate/log stress intensity factor range form: $da/dN = C\Delta K^m$, and showed a clear threshold region at $\Delta K = 7$ to 9 $MN/m^{3/2}$ which did not vary greatly with test conditions (Figure 8). The threshold values were also similar to those found for unirradiated PE16 for the same test temperatures. The wear damage and stresses developed during tiebar vibration are such that the ΔK in service will be far below the threshold value and therefore it was conclusively demonstrated that fatigue failure or fatigue crack formation could not occur during irradiation, for fuel of the burnup studied in this investigation. The absence of irradiation embrittlement in the higher temperature tests is to be expected since it is well known that this effect is time dependent, and only appears in creep-fatigue tests or low frequency fatigue tests, presumably because growth of inert gas bubbles requires diffusion. At a test frequency of 10 Hz there will be insufficient time for significant diffusion to occur during a fatigue cycle. In the lowest temperature tests (irradiated and tested at 350°C) radiation hardening was present, as shown by a markedly increased proof stress, and here the microstructural changes caused by irradiation, such as dislocation loop formation, may be expected to influence the crack propagation characteristics.

Post Test Examination

Post test metallographic examination showed that there were indeed quite marked changes in the fracture characteristics, notably a change to a strongly developed crystallographic mode of fracture (Figure 9), with frequent crack branching. This type of fracture is often associated with dislocation channelling and radiation softening, most clearly seen in fast reactor irradiations of stainless steels. The fracture surface as a result took on a very rough appearance and it is likely that roughness-induced crack closure played a part in causing the observed threshold effect. In tests at more elevated temperatures, 600°C and 700°C, the fracture surfaces were not rough since radiation damage is absent under these conditions, but oxide layers had formed which instead could be responsible for oxide-induced closure and the threshold effect found in these tests.

High Velocity Testing Facility

Besides fuel performance during irradiation, there are also safety case issues associated with transporting and handling spent fuel and in particular, the effects of fuel drops, flask drops or other hypothetical accident conditions. Under these circumstances information on the effects of impact on the fuel is useful and so the existing shielded Instron servohydraulic testing machine is being provided with a second actuator which

is capable of speeds of 25 m/s and a maximum force capacity of 20kN, and providing a kinetic energy of 2kJ for impact tests with a working stroke of 200mm. The actuator is fitted with twin 1000 l/min Moog valves for the impact test speeds and a 40 l/min valve for ordinary low speed tests, and is operated under full closed loop servo control over its whole range of speeds.

References

1. Hofman P and Spino J. Journal of Nuclear Materials vol.107 (1982) pp.297-310

2. Dakin J S. American Nuclear Soc. Int. Topical Meeting on LWR Fuel Performance West Palm Beach, Florida, 1994. pp.601-608

3. Douglas J A M and Gravenor J G. ASTM STP 1175 (1993) pp.679-695

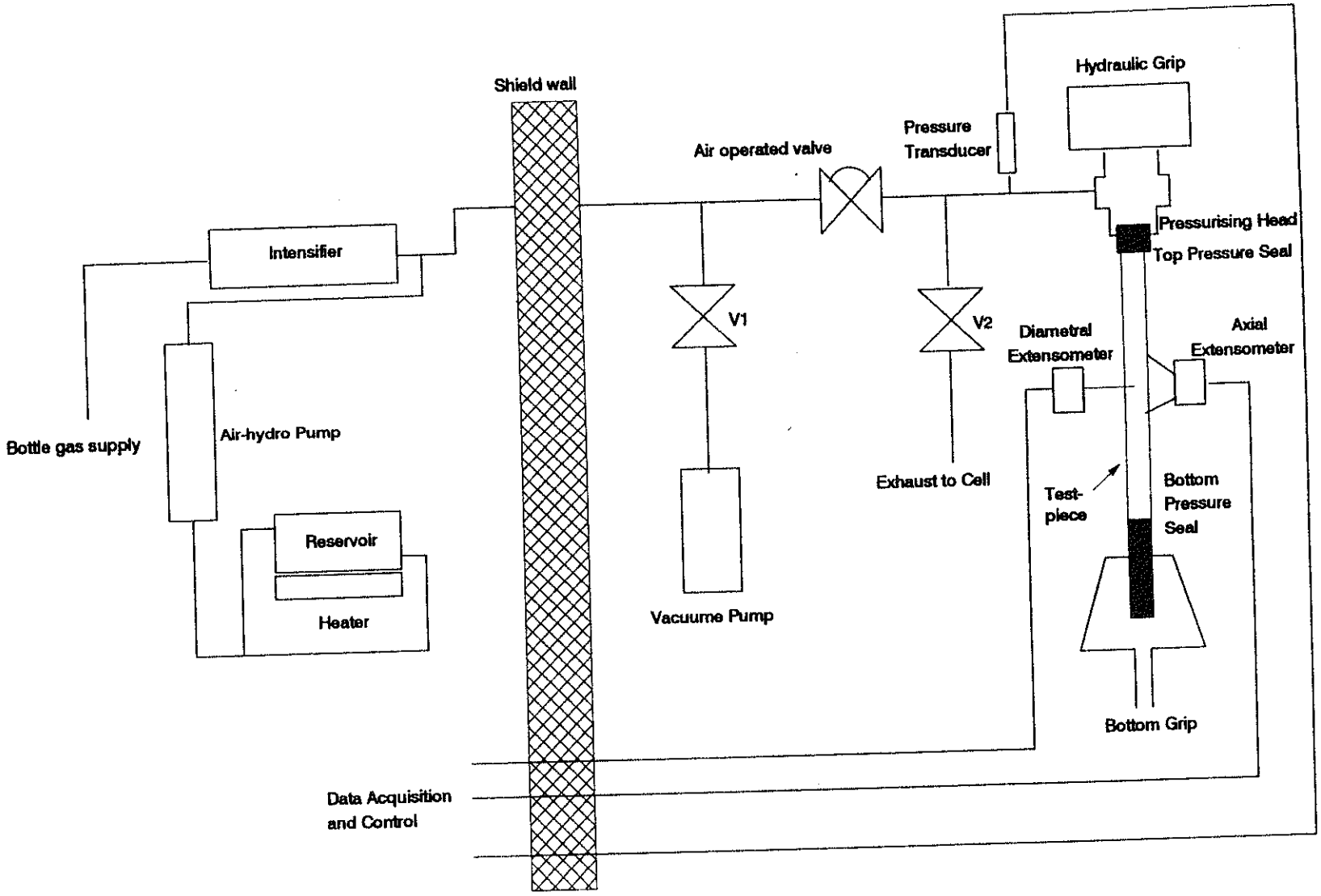

Figure 1. Diagram showing the biaxial test facility.

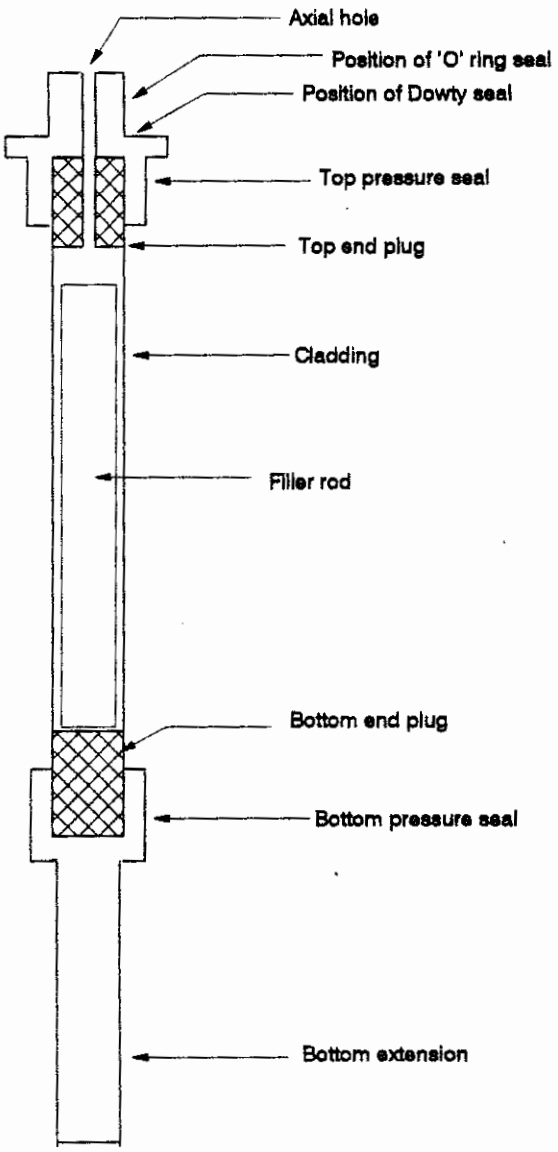

Figure 2. A typical biaxial testpiece.

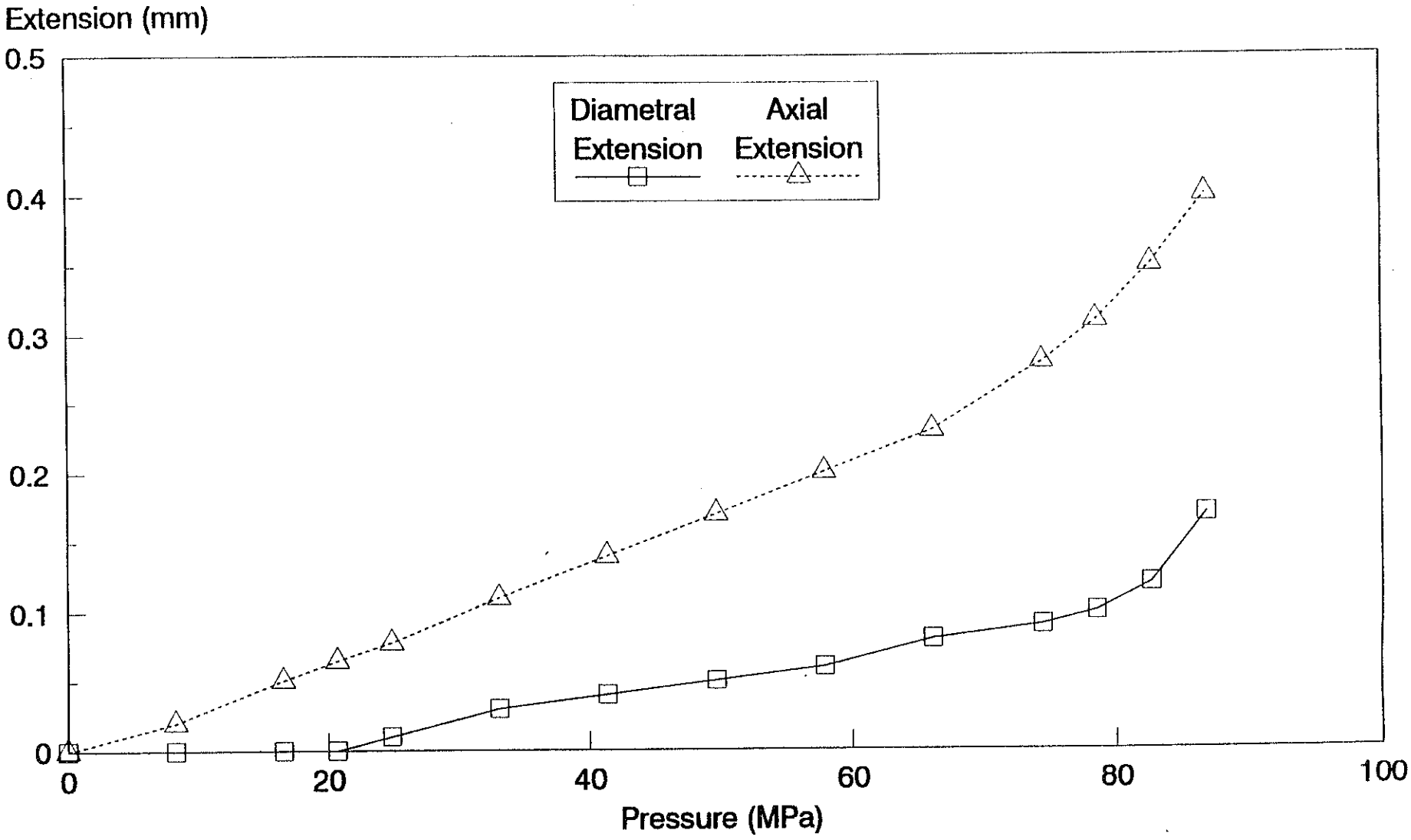

FIGURE 3: Hoop stress/axial stress = 0.8

FIGURE 4(a): Schematic of the test facility.

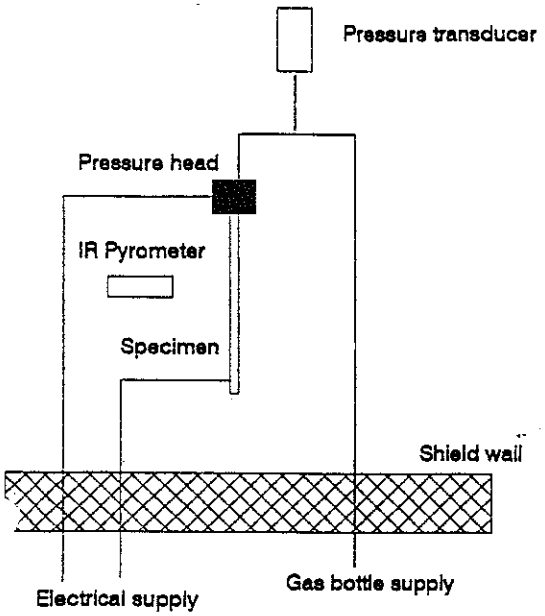

FIGURE 4(b): The iodine carrier.

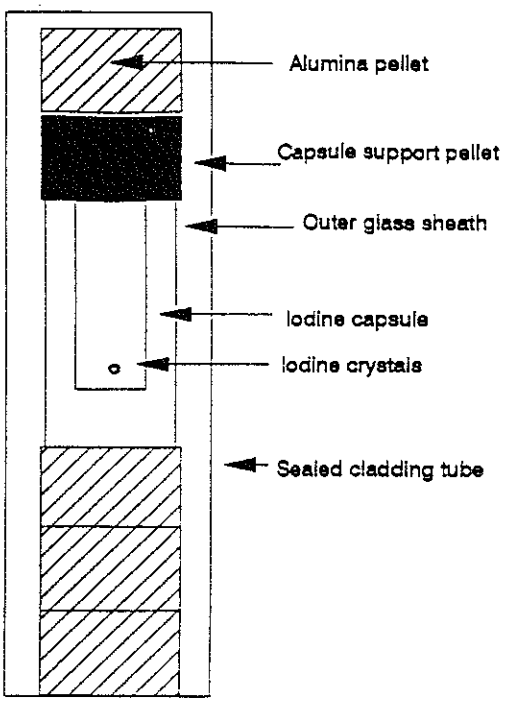

FIGURE 5: Variation of diametral strain at burst with iodine concentration for unirradiated cladding tests at 600°C.

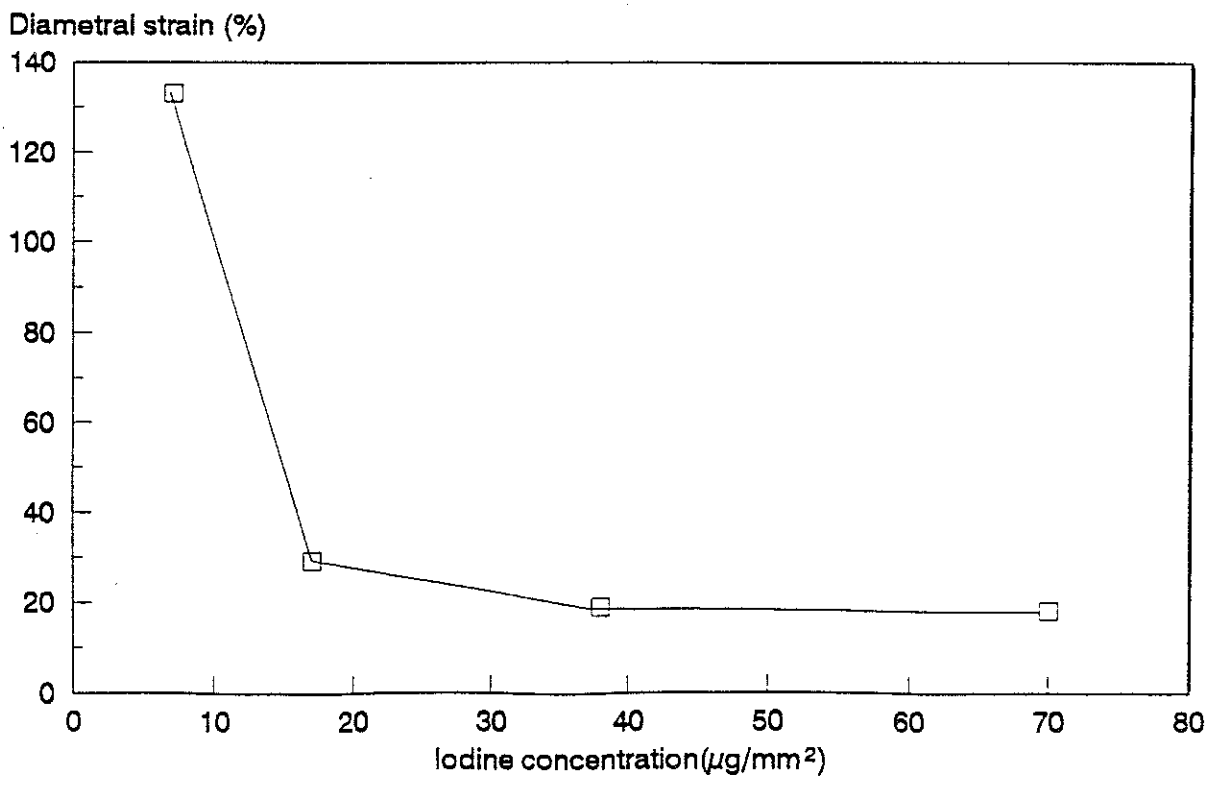

FIGURE 6: Creep curves for irradiated cladding at 600°C.

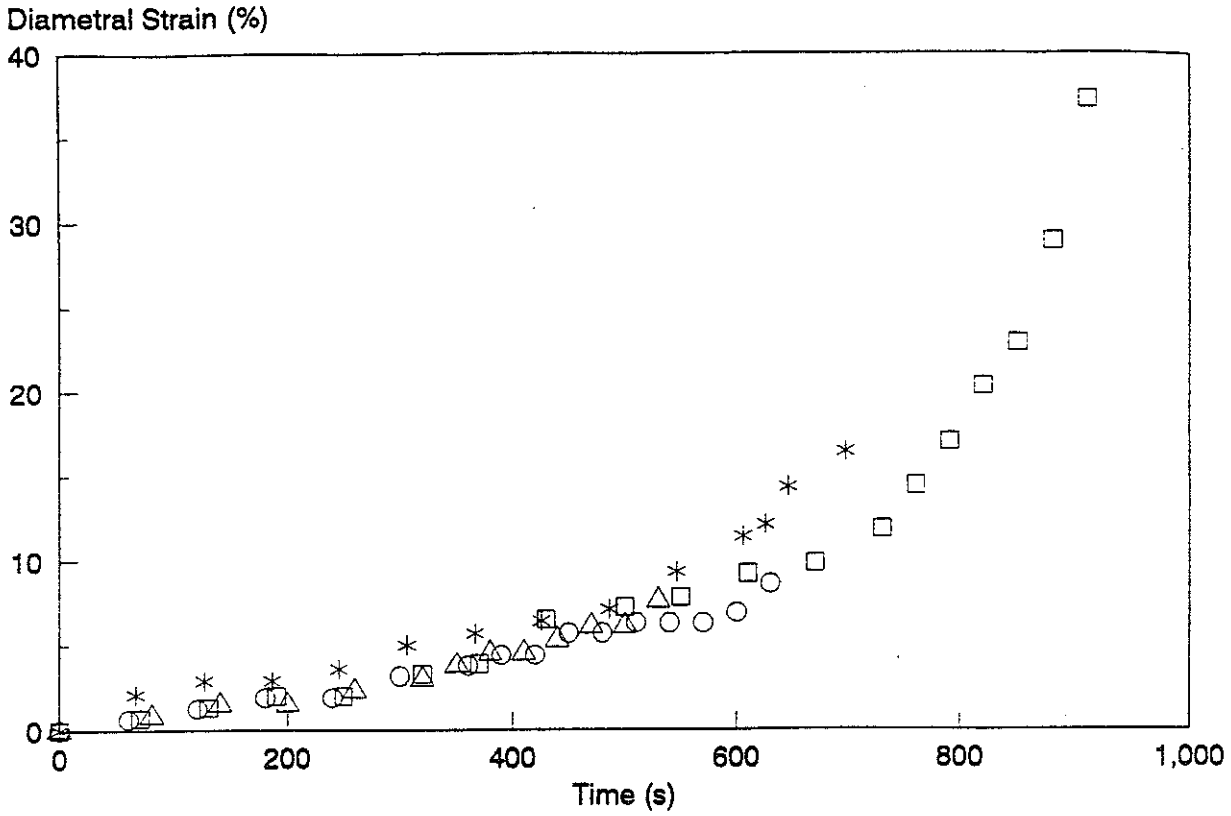

FIGURE 7: Variation of diametral strain at burst with iodine concentration for irradiated tests.

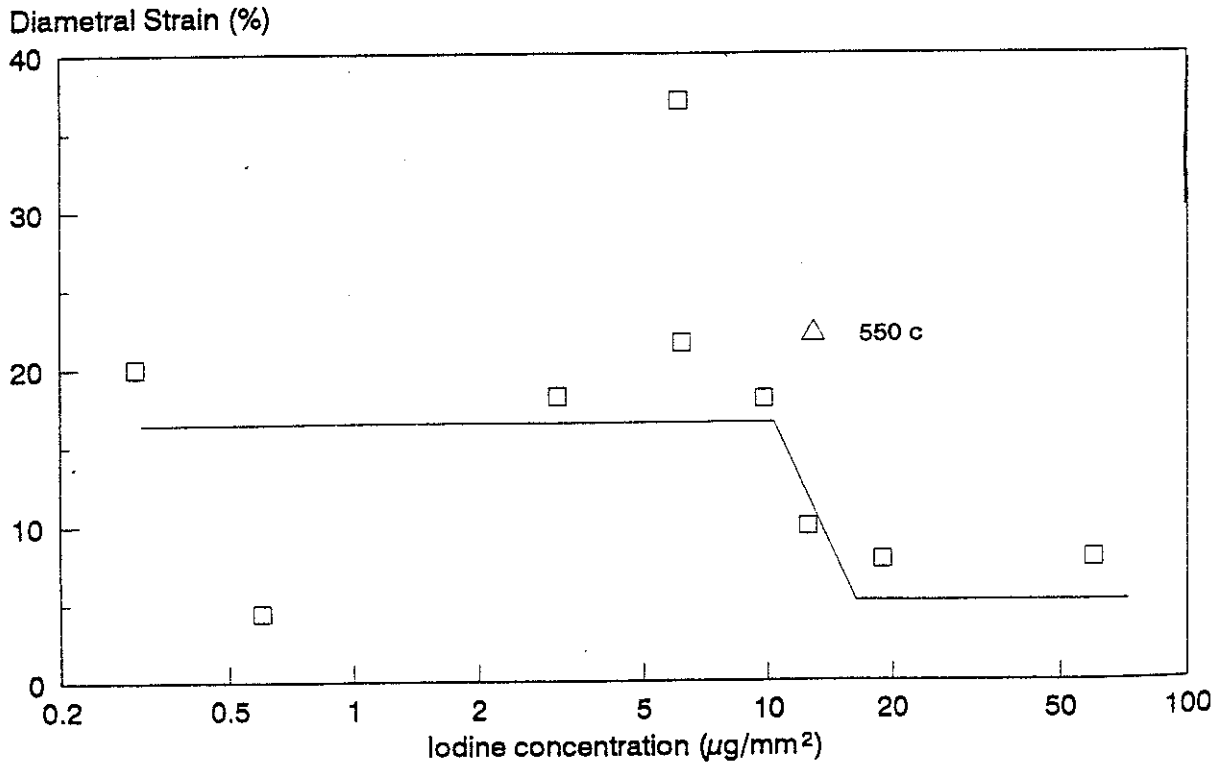

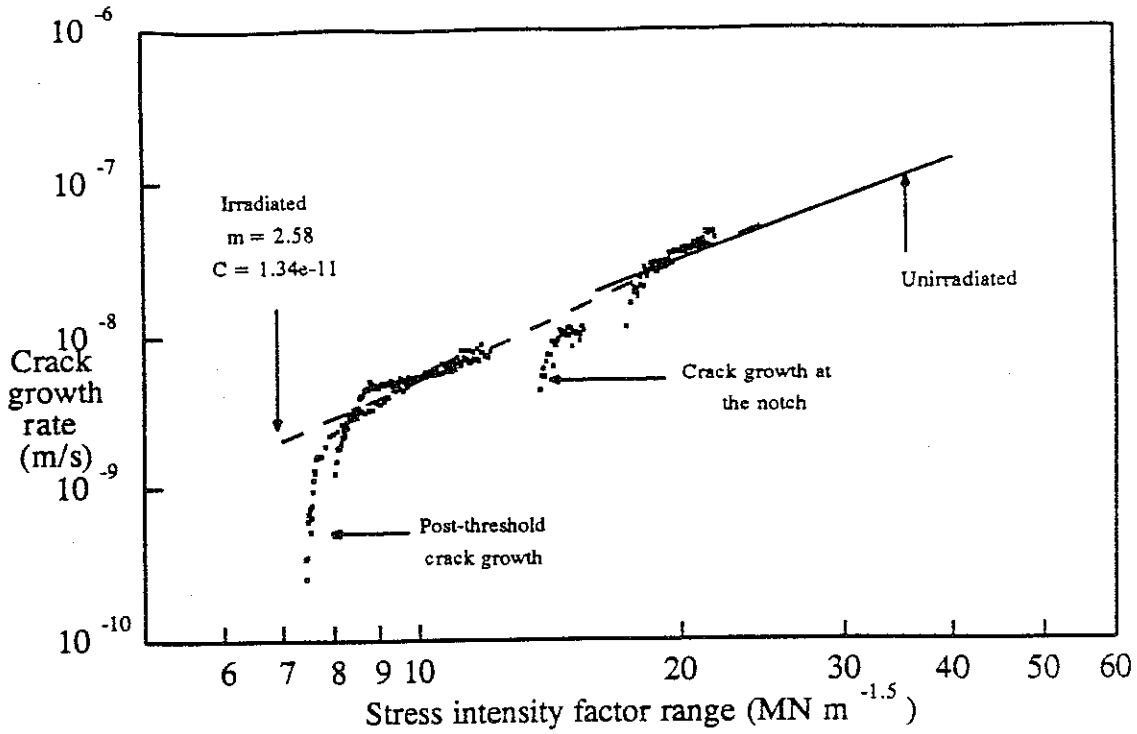

FIGURE 8(a): Crack growth data at 350°C for two fatigue tests.

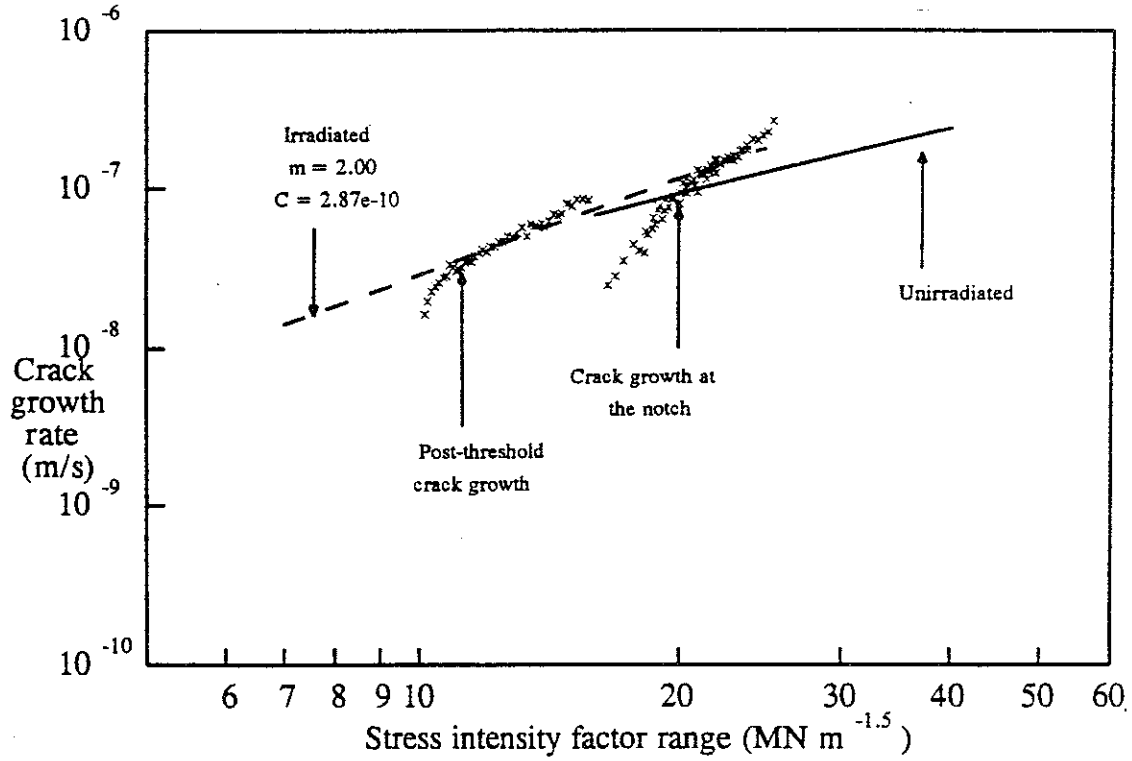

FIGURE 8(b): Crack growth data at 500°C.

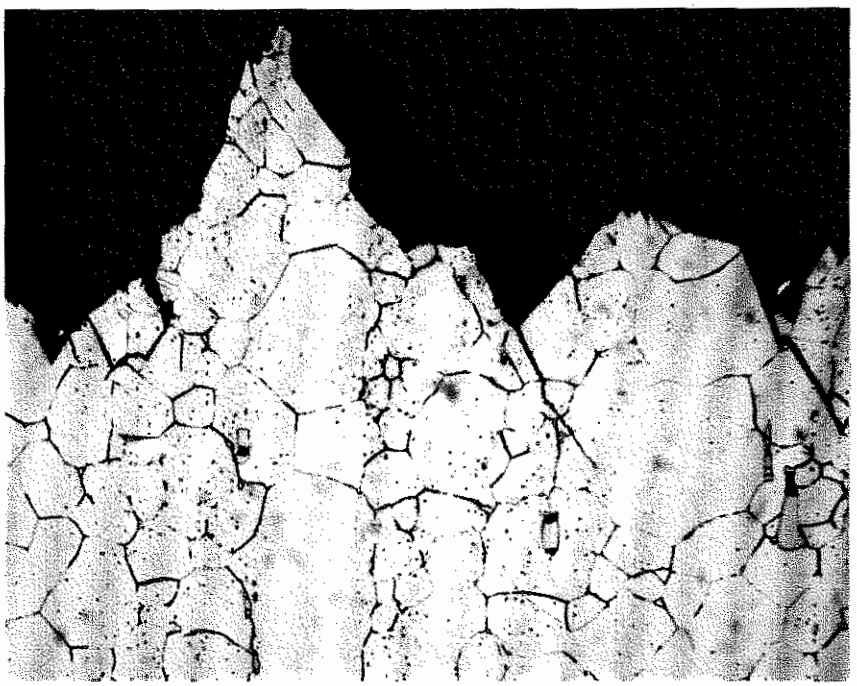

FIGURE 9: Crystallographic fracture, test at 350°C (x530).